

# A push in the right direction: exploring the role of Zealandia collision in Eocene Pacific-Australia plate motion changes

Dr. Dan Sandiford<sup>1</sup>, Peter Graham Betts<sup>1</sup>, Joanne M Whittaker<sup>1</sup>, and Louis Moresi<sup>1</sup>

<sup>1</sup>Affiliation not available

February 28, 2024



16 **Abstract**

17 The Pacific Plate underwent a significant change in motion during the early Eocene.  
 18 This change has been linked to plate boundary reconfiguration, particularly in relation  
 19 to subduction margins. The reconfiguration also resulted in a new Pacific-Australian plate  
 20 boundary section transecting Zealandia. Following the Eocene transition, the relative  
 21 rotation axis was located within continental Zealandia, and it has been hypothesized that  
 22 this region acted as a pivot point. Here we investigate the extent to which collision re-  
 23 sistance along the intra-continental Zealandia margin (length  $\sim 1000$  km) might have  
 24 impacted the motion of the Pacific Plate, which is characterised by trench lengths more  
 25 than an order of magnitude greater. We first highlight the relatively large radial com-  
 26 ponent in the Pacific Plate absolute rotation during the period ca. 47-32 Ma (i.e. the  
 27 spin around the plate centroid axis). We then consider how parameterised plate bound-  
 28 ary forces impact the tangential and radial components of the net torque (i.e. the fic-  
 29 titious and true torque components). We show that during this period, both the Zealan-  
 30 dia and Izu-Bonin-Marianas (IBM) margins of the Pacific Plate were well-oriented in terms  
 31 of partitioning boundary normal forces into counter-clockwise (CCW) radial torques. This  
 32 analysis is supported by results from recent global-scale numerical models. The role of  
 33 Zealandia cannot be established unambiguously, based on our analysis, but effects can  
 34 be quantified under different assumptions. Collision resistance along the Zealandia mar-  
 35 gin could plausibly constitute a ‘first order’ effect on Eocene Pacific Plate rotation, al-  
 36 beit only on the radial component.

37 **1 Approach and context of study**

38 This study is motivated by questions relating to the motion of the Pacific and Aus-  
 39 tralian plates during the period of significant reorganisation of plate motions (ca. 50 Ma),  
 40 which we refer to as the ‘Eocene transition’ (Whittaker et al., 2007). The change in Pa-  
 41 cific Plate motion at this time is associated with the prominent bend in the Hawaii-Emperor  
 42 Seamount Chain (Morgan, 1972; Hu et al., 2022b). Fig. 1 shows the tectonic configu-  
 43 ration, before (57 Ma) and shortly after (47 Ma) the Eocene transition, where the west-  
 44 wards change in Pacific Plate motion can be identified in the orientation of velocity vec-  
 45 tors. The change in absolute Pacific Plate motion has predominately been attributed to  
 46 the evolution of subduction margins, including cessation of Izanagi Plate subduction and  
 47 subduction of the Izanagi-Pacific Ridge, subduction initiation (e.g. the Izu-Bonin-Marianas,  
 48 or IBM margin) and subduction polarity reversal (Whittaker et al., 2007; Wessel & Kroenke,  
 49 2008; Faccenna et al., 2012; Sutherland et al., 2017; Hu et al., 2022b). In particular, the  
 50 initiation of the IBM margin has been identified as a key event (Sutherland et al., 2017;  
 51 Hu et al., 2022b; Gurnis, 2023).

52 Along with changes in Pacific Plate subduction margins, the Eocene transition also  
 53 involved reconfiguration of Pacific-Australian plate boundary as well as relative motion  
 54 between these plates. Tasman Sea spreading ceased at about 50 Ma, and the Pacific-Australian  
 55 plate boundary relocated onto a fault zone transecting the rifted Gondwanan fragment  
 56 of Zealandia (Gaina et al., 1998). We refer to the intra-continental part of this bound-  
 57 ary as the ‘Zealandia margin’, as shown in the upper right panel of Fig. 2. Although this  
 58 fault zone is inferred to significantly predate the Eocene transition (Lamb et al., 2016),  
 59 the critical change at this time was the transfer of Pacific-Australian relative motion onto  
 60 this system.

61 During the period ca. 45-30 Ma (and potentially somewhat earlier) the Euler pole  
 62 of relative rotation between the Pacific and Australian Plates, was situated within or close  
 63 to Zealandia (Sutherland, 1995; Keller, 2005). Fig. 2b shows two relative Euler pole lo-  
 64 cations inferred at times near the Eocene transition. The black circle is the 47 Ma pole  
 65 from Müller et al. (2016), and is derived from a plate circuit (relative motion model) through  
 66 the West-Antarctic (W-ANT) and Antarctic (ANT) plates. The black cross is the 45 Ma

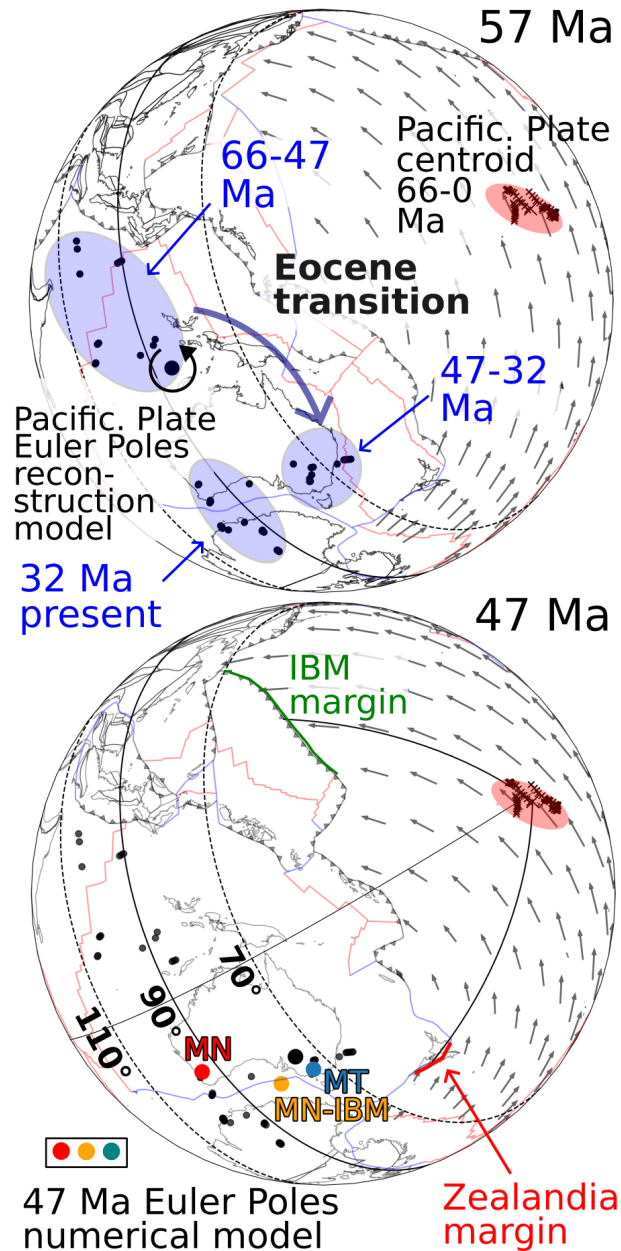


**Figure 1.** Tectonic configuration of the SW Pacific, shown before (57 Ma) and after (47 Ma) the Eocene transition. All tectonic features are based on the plate reconstruction model of Müller et al. (2016), with alternative north Pacific subduction margins as presented in Hu et al. (2022b). Cenozoic locations of Pacific Plate Euler poles are shown with black circles, from the same reconstruction models. The larger black circle shows the Euler pole at the reconstruction time; arrow shows the CCW rotation sense. Euler poles and plate velocity arrows reflect Pacific Plate rotations in the absolute reference frame described in Müller et al. (2016). A great circle at an angle of 90° to the Pacific Plate centroid is shown with a solid black line, as labelled. Three distinct clusters in Euler pole locations can be identified, as highlighted by blue regions and labels in the top panel. The Eocene transition (indicated by the blue arrow) corresponds to a migration of the Euler pole location towards the southeast, as well as a  $\sim 25^\circ$  migration towards the Pacific Plate centroid. Centroid locations at 1 Myr intervals throughout the Cenozoic are shown with black crosses, and highlighted in the red region. In the lower panel, the red, blue and yellow circles show Pacific Plate Euler poles from 3 global numerical models presented in Hu et al. (2022b).

67 Euler pole from Sutherland (1995), which is the earliest direct estimate of relative motion  
 68 determined from spreading features in the Emerald Basin (the location of which is  
 69 shown in the lower right panel of Fig. 2). The pole locates in central Zealandia, close  
 70 to the inferred western limit of the underthrust Hikurangi Plateau (HP).

71 The Hikurangi Plateau is thought to play a central role in the evolution of Zealandia  
 72 (Reyners, 2013; Mortimer, 2018). This region emerged as part of the Ontong-Java  
 73 large igneous province at ca. 120 Ma (Mahoney et al., 1993), later colliding with the Gond-  
 74 wanan arc and underthrusting the continental margin. Back arc spreading commenced  
 75 at around 90 Ma, leading to the opening of the Tasman Sea and the progressive rifting  
 76 of Zealandia, including the underthrust HP, away from Gondwana (Gaina et al., 1998).  
 77 This phase is shown in the upper left panel of Fig. 2. In relation to Pacific-Australian  
 78 plate motion following the Eocene transition, Reyners (2013) has proposed that “resistance  
 79 of the [Hikurangi] plateau to subduction had a first-order effect”. In particular,  
 80 “the western tip of the [Hikurangi] plateau appears to have acted as a pivot point on the  
 81 plate boundary” (see also Eberhart-Phillips et al. (2018)).

82 In terms of the absolute motion of Pacific Plate, the Eocene transition comprised  
 83 significant changes in, respectively, the tangential and radial components of the rotation  
 84 vector (as we show in Section 2). Moreover, changes in both of these components facilitate  
 85 an overall shift of absolute Pacific Plate Euler poles toward Zealandia. In this way,  
 86 we highlight the potential connection between changes in absolute Pacific Plate motion,  
 87 as well as its motion relative to the Australian Plate. In sections 3&4 we investigate the  
 88 extent to which forces acting along the Zealandia margin could have impacted this change  
 89 in (absolute) Pacific Plate motion. This represents an attempt to quantitatively evaluate  
 90 the hypothesis of Reyners (2013). Specifically, we evaluate the relative effects of a  
 91 putative collision resistance at the Zealandia margin, compared with Pacific Plate margin  
 92 subduction forces. While this type of geometric analysis has an extensive history in  
 93 the literature (Forsyth & Uyeda, 1975; Becker & O’Connell, 2001; Faccenna et al., 2012),  
 94 the novelty here is to investigate how such margin-normal forces would contribute to what  
 95 we describe as the tangential and radial components of the net torque.

96 The context and approach of our study is informed by the idea that while plates  
 97 are driven/resisted by a range of mechanisms, not all of these are capable of evolving rapidly  
 98 (Faccenna et al., 2012; Colli et al., 2014; Hu et al., 2022b). For instance, plates may be  
 99 coupled to a whole-mantle flow through basal shear as well as forces due to dynamic topog-  
 100 raphy (Steinberger et al., 2001). While such contributions are thought to play a significant  
 101 role in terms of Cenozoic Pacific Plate dynamics, they are also expected to evolve  
 102 slowly (Steinberger et al., 2001; Faccenna et al., 2012; Stotz et al., 2018). On the other  
 103 hand, forces such as direct slab pull, and collision resistance, are viewed as being capable  
 104 of evolving rapidly (England & Molnar, 2022; Hu et al., 2022b). The implication of  
 105 these points is that torques due to subduction and collision represent only a partial description  
 106 of the overall plate equilibrium. This has important implications for how we  
 107 interpret comparisons between torques and plate rotation vectors. We pick up on this  
 108 issue in Section 4. We will also address the limitations of our simple geometric analysis,  
 109 by considering results from recent global-scale numerical models (Hu et al., 2022b).

## 110 2 Plate motion models

111 In this study we use a global plate reconstruction model (Müller et al., 2016) to  
 112 address both the relative and absolute rotations of the Pacific and Australian plates. By  
 113 absolute rotations, we are referring both to the model of relative motions as well as the  
 114 reference frame to which the relative motion model is anchored. Following Müller et al.  
 115 (2016), the relative motion model is fixed (for the past 100 Ma) to a global moving hot-  
 116 spot model (Torsvik et al., 2008). The evolution of Pacific Plate Euler poles in the Müller  
 117 et al. (2016) model is shown in Fig. 1, while additional reference frames are shown in

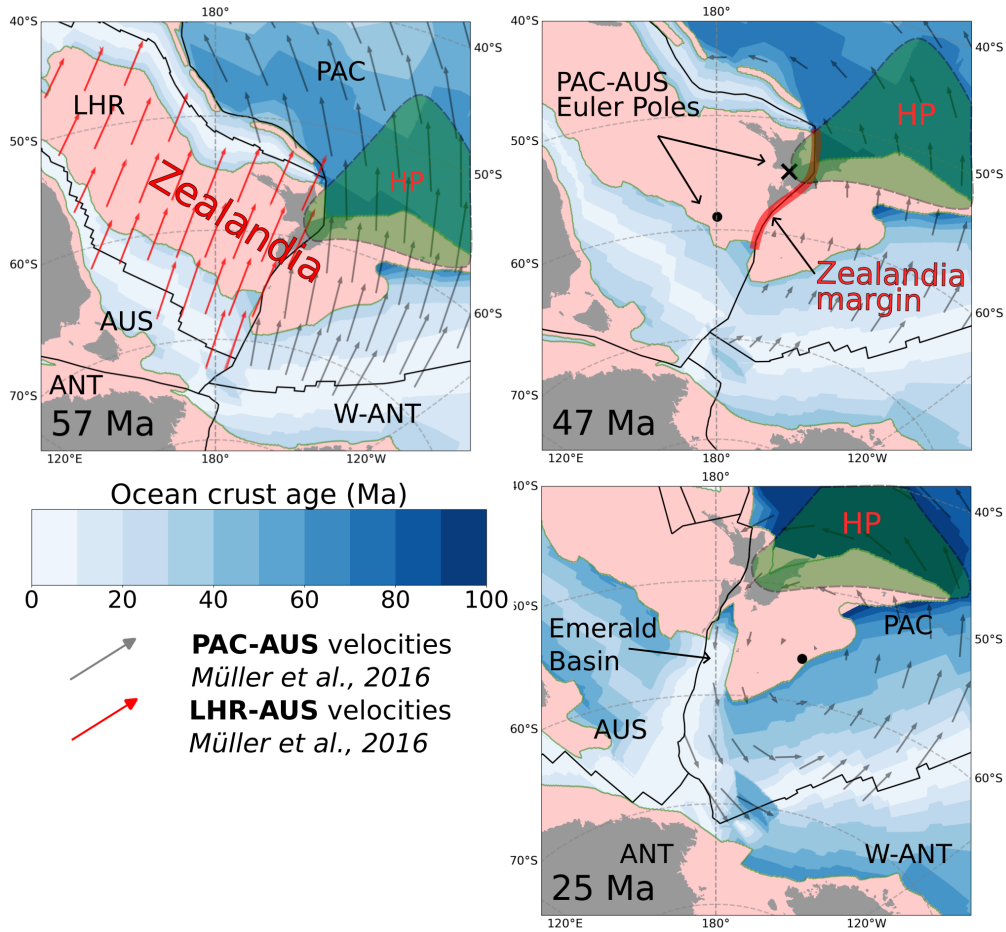


**Figure 2.** Cenozoic evolution of the Pacific-Australia plate boundary system based on the plate reconstruction of Müller et al. (2016); geometries are shown relative to the absolute reference frame. Pink regions represent approximate extents of continental crust; grey regions are reconstructions of current-day coastlines; green region is the approximate extent of the Hikurangi Plateau (HP), including the parts inferred to be underthrust beneath Zealandia (see Reyners (2013) for geophysical constraints). Solid black lines show plate boundaries from Müller et al. (2016). Black labels in the upper left panel are abbreviations for the plates, as discussed in the main text. The Zealandia margin – the intra-continental part of the Pacific-Australian plate boundary – is highlighted with red. The black velocity arrows show the rotation of the Pacific Plate relative to a stationary Australian Plate (red arrows show the same for the Lord Howe Rise Plate). In the top left panel (57 Ma) Zealandia straddles the Pacific and LHR plates, which are both rifting north from Gondwana, along with minor relative rotation. The Euler poles for Pacific-Australian relative motion, from Müller et al. (2016), are shown with the black circles. The black cross in the upper right is the 45 Ma Euler pole estimated by Sutherland (1995) from spreading features in the Emerald Basin. Lower right panel shows the incipient phase of Alpine Fault System.

118 Supplementary Fig. S1, including a fixed Pacific hotspot frame (Wessel & Kronke, 2008).  
 119 While the overall trajectories of these poles show significant similarity, there are non-  
 120 trivial differences in timing. These differences are more obvious when we consider the  
 121 decomposition of the rotation vectors at the plate centroid (as shown in Fig. S2, and dis-  
 122 cussed later in this Section). Since there appears to be general consensus for moving Pa-  
 123 cific hotspots (Steinberger, 2000; Torsvik et al., 2008), our analysis focuses on absolute  
 124 plate motions models based on global moving hotspot frames (Müller et al., 2016; Torsvik  
 125 et al., 2008).

126 In terms of trying to quantify the role of tectonic forces in driving changes in plate  
 127 motion, we focus primarily on the changes expressed in the absolute motion of Pacific  
 128 Plate (for reasons that are elaborated throughout the manuscript). The Cenozoic ab-  
 129 solute rotation poles of the Pacific Plate are shown with black circles in Fig. 1. Three  
 130 distinct clusters in pole locations can be identified, as highlighted by blue regions and  
 131 labels. An important observation, particularly in the context of this study, is that dur-  
 132 ing the Eocene transition, Pacific Plate Euler poles shift much closer to Zealandia. This  
 133 suggests that changes in the absolute motion of the Pacific Plate partly facilitated the  
 134 corresponding change in the locations of the relative (Pacific-Australian) poles, such that  
 135 the latter were located within or close to Zealandia throughout the pivot period. This  
 136 relationship cannot simply be assumed at the outset, as the relative Euler poles could  
 137 (in principle) be completely controlled by changes in the Australian Plate absolute mo-  
 138 tion. This does not seem to be the case. These connections also underpin our focus on  
 139 Pacific Plate absolute motion throughout the remainder of the manuscript.

140 A key aspect of this study is to consider a decomposition of the plate rotations into  
 141 ‘radial’ and ‘tangential’ components. The radial component is the spin around an axis  
 142 ( $\hat{r}_c$ ) that points radially outwards at the plate centroid. The decomposition of the plate  
 143 rotation vector ( $\vec{\omega}$ ) can simply be expressed as:

$$\begin{aligned}\vec{\omega}_{\text{rad}} &= \vec{\omega} \cdot \hat{r}_c \\ \vec{\omega}_{\text{tan}} &= \vec{\omega} - \vec{\omega}_{\text{rad}}\end{aligned}\tag{1}$$

144 Note that when a plate rotation is purely tangential (at the centroid), the rotation  
 145 axis is orthogonal to the centroid vector, and hence the Euler pole of the rotation lies  
 146 at  $90^\circ$  from the plate centroid; the finite rotation at the centroid is then a great circle  
 147 arc. In contrast, the plate rotation is purely radial when the Euler pole lies at the plate  
 148 centroid, in which case the plate spins about the radial axis.

149 The radial and tangential rotation components expressed in Eq. 1 will clearly de-  
 150 pend on the magnitude of the rotation vector  $\vec{\omega}$ . However, if we consider only the ori-  
 151 entation of  $\vec{\omega}$ , (i.e.  $\hat{\omega}$ ), then the radial component of rotation can be approximated as  
 152 an angle:

$$\hat{\omega}_{\text{rad}} = \cos(\gamma) = \sin\left(\frac{\pi}{2} - \gamma\right) \approx \left(\frac{\pi}{2} - \gamma\right)\tag{2}$$

153 where  $\gamma$  is the angle between the Euler pole and the centroid, and the small an-  
 154 gle approximation is made. This expression shows that the relative amount of plate ra-  
 155 dial rotation, has an intuitive geographic representation, being the angle between the Eu-  
 156 ler pole and a great circle drawn at  $90^\circ$  from the centroid. Supplementary Fig. S3 shows  
 157 a comparison between the approximation of the radial component of Pacific Plate ro-  
 158 tation ( $\frac{\pi}{2} - \gamma$ ) and the true radial component ( $\vec{\omega}_{\text{rad}}$ , in units of  $^\circ/100$  Ma). Note that  
 159 with this choice of units, the magnitude of the Pacific Plate radial component, in both  
 160 the true and approximate measure, are very similar.

161 Fig. 3 shows the Cenozoic evolution of Pacific Plate rotation, decomposed into ra-  
162 dial and tangential components. The tangential component of the rotation has addition-  
163 ally been decomposed into an azimuth (Fig. 3A) and a magnitude (Fig. 3B) at the cen-  
164 troid. This decomposition shows that the Eocene transition (ca. 47 Ma) involved both  
165 the (often-discussed) westwards change in the rotation azimuth, as well as a significant  
166 (CCW) change in the radial rotation component (Fig. 3C). In fact, the period of 47-32  
167 Ma is associated with the largest Pacific Plate radial rotation component of any time dur-  
168 ing the Cenozoic. This period of higher radial rotation overlaps broadly the same inter-  
169 val (ca. 45-30 Ma) where estimates of Pacific-Australian relative motion place the ro-  
170 tation pole within Zealandia (Sutherland, 1995). Based on this association, we refer to  
171 this interval as the ‘pivot period’. Following this period, the (absolute) Pacific Plate ra-  
172 dial rotation component rapidly reverted to weakly CW, and remained relatively sta-  
173 ble until about 10 Ma, when a further  $\sim 5^\circ$  (CW) increase occurred. In the following  
174 section we analyse how plate boundary normal forces contribute to the torque compo-  
175 nents that may drive such changes in plate rotation. This begins with a general devel-  
176 opment, which is then applied to Pacific Plate margins in the Cenozoic.

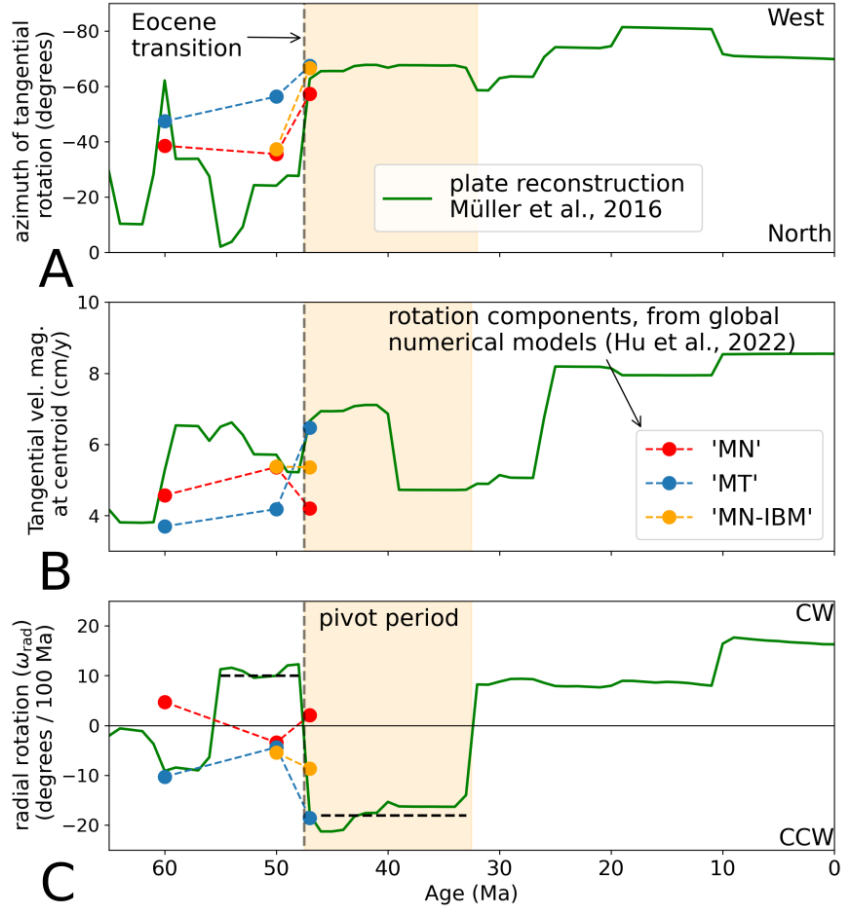


**Figure 3.** Cenozoic Pacific Plate motion trends, relative to hotspot reference frames, evaluated at the Pacific Plate centroid, based on plate reconstruction model if (Müller et al., 2016). As discussed in the main text, the Figure shows a decomposition of the plate rotation vector into: A) the azimuth of the velocity at the centroid; B) the magnitude of the tangential part of the rotation vector; and C) the radial rotation component. In this study, the Eocene transition is defined as the time associated with the significant (westwards) azimuthal change in Pacific Plate motion. In the plate reconstructions analysed in this study, the Eocene transition occurs at 47 Ma, although a window of at least several million years is suggested by previous studies (Whittaker et al., 2007; O’Connor et al., 2015). The ‘pivot period’ (ca. 47 - 32 Ma) is defined as the duration of relatively strong CCW radial rotation on the Pacific Plate; this interval largely coincides with the period in which the relative Pacific-Australian Euler poles were located within or close to Zealandia. The colored circles show Pacific Plate rotation components, as predicted in global-scale numerical models (Hu et al., 2022b). These numerical model results are discussed in Section 5.

### 3 Theory and methods

#### 3.1 Torques due to plate boundary force

Because plate motion is restricted to the surface of a sphere, the 6 degrees of freedom that apply to rigid body motion, can be reduced to 3 rotational components (Forsyth & Uyeda, 1975; Bird et al., 2008). The equilibrium problem is then to understand the balance of torques that give rise to observed rotations. For plate motions, rotations are commonly expressed in terms of a rotation axis (or Euler pole) and angular velocity, or simply a rotation vector ( $\vec{\omega}$ ).

The rotations and torques are naturally described with respect to the center of the Earth, and hence the radius of the Earth enters the description as the moment arm length. For instance, in terms of parameterised plate boundary forces (Forsyth & Uyeda, 1975; Becker & O’Connell, 2001), the torque vector component due to a plate boundary normal force, over a small section of trench, may be written as:

$$d\vec{\tau} = F_n(\vec{r}_0 \times \hat{n})dl \quad (3)$$

Where  $F_n$  is the (scalar) normal force density (force per unit length, expressed in this study in units of TN/m),  $\hat{n}$  is a unit vector in the local tangent plane that is normal to the plate boundary, and  $\vec{r}_0$  is the radius vector that points to the location of the plate boundary. The total torque due to plate boundary normal forces is:

$$\vec{\tau}_{\text{net}} = \sum F_n(\vec{r}_0 \times \hat{n})dl \quad (4)$$

Eq. 4 represents a typical description used to investigate mechanical equilibrium of rigid plates on a sphere (Forsyth & Uyeda, 1975; Becker & O’Connell, 2001). However, this description tends to obscure an important aspect of the mechanics, which is that the torque vector described by Eqs. 3 and 4, conflates two kinds of torques. The distinction between these types of torques is closely related to the more familiar case of the motion of a solid object constrained to a planar surface. The mechanical descriptions converge for very small plates, which are approximately planar. Fig. 4 attempts to clarify these relationships. We will hereafter condense the notation by denoting the point force along a small boundary increment ( $dl$ ) as  $\vec{F}_n = F_n dl \hat{n}$ , and dropping the differential symbol, so that Eq. 3 can be written as:

$$\vec{\tau} = \vec{r}_0 \times \vec{F}_n \quad (5)$$

Fig. 4 shows the effect of an arbitrary point force  $\vec{F}_n$  acting on a square plate confined to (a) a planar surface and (b) the surface of a sphere. Note that in both cases the  $z$  axis is aligned with the vertical direction at the centroid of the plate. The line that connects the centroid to the point force location, is referred to as the centroid direction. The centroid directions are shown with the solid blue line in (a) and the solid blue arc in (b). Note that the centroid direction is parallel to the  $y$  axis (in a) and lies in the  $y$ - $z$  plane (in b). In the latter case, ‘parallel to the centroid direction’, means parallel to the local orientation of the centroid direction arc, i.e. a vector in the local tangent plane.

In each case a point force, represented by a green arrow, acts at the corner of the square plate. This point force is parallel to the direction given by the dashed edge, and hence normal to the adjacent edge. The point force vector has been decomposed into components that are parallel (blue) and orthogonal (brown) to the centroid direction. In the planar case (a), a torque arises because the point force (green vector) has a component that is orthogonal centroid direction; this orthogonal component of the point force is given

218 by  $|\vec{F}_n| \sin(\theta)$ , and the torque is given by  $\vec{r} \times \vec{F}_n$ , or  $-|\vec{F}_n||\vec{r}| \sin(\theta) \hat{z}$ . However this or-  
 219 thogonal component also contributes to the net (linear) force on the plate. We use the  
 220 brown arrow to signify the contribution (of the orthogonal component of the point force)  
 221 to the linear force, and the black arrow to signify the contribution to the torque.

222 Now we consider the extension of this behavior to the spherical case. In the con-  
 223 ventional analysis of plate boundary forces, a point force  $\vec{F}_n$ , such as is shown with the  
 224 green arrow in (b), will be assumed to contribute to a driving torque  $\tau$  (as in Eqs. 3 or  
 225 5). Similar to the foregoing analysis, we can decompose this torque in such a way as to  
 226 highlight the contributions of the force components that act parallel and orthogonal to  
 227 the centroid direction.

228 Consider first the component of the torque associated with the force parallel to the  
 229 centroid direction (blue arrow). For the configuration shown in (b), this component of  
 230 the torque vector is parallel to the  $x$  axis. The moment arm length is  $r_0$ , it has no de-  
 231 pendence on the location of the point force (which is analogous to the planar case). This  
 232 component of the driving torque produces purely tangential motion at the centroid, be-  
 233 cause  $\hat{r}_c \times \hat{x}$  is tangent to the surface, where  $\hat{r}_c$  is a unit vector that points radially out-  
 234 ward at the centroid. For the configuration shown in (b),  $\hat{r}_c \equiv \hat{z}$ .

235 Next consider the component of the torque in (b) that acts in the  $z$  direction (which  
 236 in this configuration is also referred to as the centroid direction  $\hat{r}_c$ ). This represents the  
 237 component of a torque vector that tends to spin the plate around the centroid. We refer  
 238 to this as the radial component of the torque due to  $\vec{F}_n$ . This radial component of  
 239 the torque has a moment arm length of  $r_0 \sin(\varphi)$  where  $\varphi$  is the angle between the cen-  
 240 troid and the boundary where the force is located. As in the planar case, this compo-  
 241 nent of the torque has an intrinsic dependence on the distance between the point force  
 242 and the centroid (or  $z$  axis). Note that in the case of a very small plate, we can use the  
 243 small angle approximation ( $\sin(\varphi) \approx \varphi$ ) in which case, the  $z$  component of the torque  
 244 depends on  $r_0 \varphi \approx y$ , i.e the torque is simply proportional to the distance from the  $z$   
 245 axis, as in the planar case.

246 The brown arrow shown in (b) is the component of the force that gives rise to the  
 247 torque component around the  $y$  axis. This also produces purely tangential motion at the  
 248 centroid. Again, this is analogous to the effect of the net linear force in (a), given by the  
 249 component of force acting orthogonal to the centroid direction. The moment arm length  
 250 is given by  $r_0 \cos(\varphi)$ , or by  $r_0$  in the small angle approximation.

251 As shown in Fig. 4, the radial and tangential components of the torque can be writ-  
 252 ten in terms of (1) the angle between the plate boundary normal and the centroid di-  
 253 rection ( $\theta$ ) and (2) the angle between the location where the point force acts and the cen-  
 254 troid ( $\varphi$ ):

$$\begin{aligned} \vec{\tau}_{\text{rad}} &= -|\vec{F}_n| r_0 \sin(\theta) \sin(\varphi) \hat{z} \\ \vec{\tau}_{\text{tan}} &= -|\vec{F}_n| r_0 \cos(\theta) \hat{x} \\ &\quad + |\vec{F}_n| r_0 \sin(\theta) \cos(\varphi) \hat{y} \end{aligned} \tag{6}$$

255 The tangential component of the torque can also be described by an equivalent force  
 256 acting at the centroid (e.g., Becker & O'Connell, 2001):

$$\vec{F}_{\text{eq}} = (\vec{\tau}_{\text{tan}} \times \hat{r}_c) / r_0 \tag{7}$$

257 Because the surface of a sphere is locally flat, the description of the spherical case  
 258 must be identical to the planar case for a small plate. This can be verified by applying

259 the small angle approximations (for  $\varphi$ ) to the tangential and radial components of the  
 260 torque, and representing the former as an equivalent force. Based on these considera-  
 261 tions we refer to the tangential and radial components of the torque vector as fictitious  
 262 and true torque components.

263 For the radial component of plate driving/resisting torques, the magnitude of the  
 264 torque depends on two aspects of the geometry: the azimuth of the plate boundary  
 265 relative to the centroid (i.e. the component of the force that is normal to the centroid di-  
 266 rection ( $\sin(\theta)$ ), and also the angle (distance) between the plate centroid and the bound-  
 267 ary ( $\sin(\varphi)$ ). Hence, plate boundary normal forces that are perpendicular to the centroid  
 268 direction, and are a long way from the centroid (i.e.  $\sin(\varphi), \sin(\theta) \rightarrow 1$ ) have the great-  
 269 est potential to impact the radial component of torque. In the following section we extend  
 270 these generic ideas to the case of the Zealandia and the IBM margin in the Eocene.

Parameter name	Type	Symbol	Units
Earth mean radius	scalar	$r_0$	km
Earth radius vector	vector	$\vec{r}_0$	km
Earth radius unit vector	vector	$\hat{r}_0$	-
Plate boundary normal vector	vector	$\hat{n}$	-
Plate boundary normal force density <sup>†</sup>	scalar	$F_n$	TN/m
Plate boundary normal point force	vector	$\vec{F}_n$	TN
Plate centroid unit vector	vector	$\hat{r}_c$	-
Angle btw $\hat{n}$ & centroid direction	scalar	$\theta$	rad.
Angle btw boundary point & centroid	scalar	$\varphi$	rad.
Rotation vector	vector	$\vec{\omega}$	$^\circ/\text{Ma}$
Radial rotation unit vector $\ddagger$	vector	$\hat{\omega}_{\text{rad}}$	$^\circ$
Angle btw centroid and Euler pole	scalar	$\gamma$	$^\circ$

**Table 1.** Quantities and symbols used in the paper. <sup>†</sup> We discuss both dimensionless and dimensional values for plate boundary normal forces. Where dimensional values are used, the units will generally be expressed as TN, or  $\text{TN m}^{-1}$ . <sup>‡</sup> See Section 4 for a description of units and how  $\hat{\omega}_{\text{rad}}$  is visualised.

### 271 3.2 Application to Pacific Plate at 47 Ma

272 We now highlight the key ideas from the previous section, in the context of the Pa-  
 273 cific Plate boundary configuration at the Eocene transition; the purpose here remains  
 274 primarily conceptual (the main results being presented in Section 4). Fig. 5 shows the  
 275 tectonic configuration at 47 Ma, rotated so that the Pacific Plate geometric centroid lies  
 276 along the  $z$  axis of a Cartesian coordinate system, and so that the arc that connects the  
 277 centroid to a point on the IBM trench lies in a plane defined by the  $y$ - $z$  axes (i.e. the cen-  
 278 troid direction, as shown with a thin blue line). This rotation places the Pacific Plate,  
 279 and the IBM margin, into a similar configuration as has been shown in the generic case  
 280 in Fig. 4b. In the right hand panel of Fig. 5, the force due to slab pull at the IBM is rep-  
 281 resented as a point force acting in a margin normal direction (shown schematically with  
 282 a green arrow). The net torque vector associated with a margin-normal point force at  
 283 the center of the IBM margin is shown with the green arrow at the centroid location. The  
 284 decomposition of the torque vector around the Cartesian axes is shown with the coloured  
 285 arrows, as discussed in the Figure caption. Importantly, one can see that the radial com-  
 286 ponent (black) is of similar magnitude to the components that contribute to the tangen-  
 287 tial torque (blue and brown).

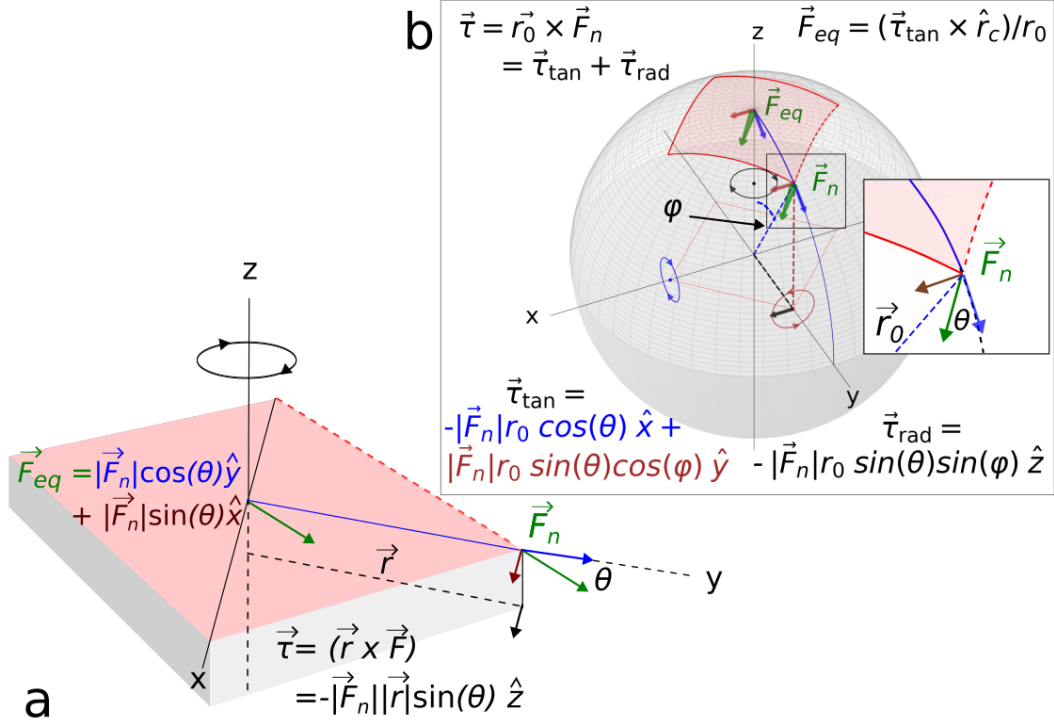


**Figure 4.** Effect of an arbitrary point force  $\vec{F}_n$  acting on a square plate confined to (a) a planar surface and (b) the surface of a sphere: (a) shows the familiar case of a point force acting on a rigid body, contributing to a net force and a torque around the center of the object.  $\vec{F}_n$  acts at the corner of the square plate, in a direction parallel to the edge of the square outlined with the dashed red line, and normal to the adjacent edge. The blue and brown arrows show the components of the force that are parallel and perpendicular to the centroid direction. The components of the net force ( $\vec{F}_{eq}$ ), and the torque ( $\tau$ ) are written as a function of  $\theta$ , the angle between the point force on the boundary and the centroid direction. For the configuration represented here,  $\theta = 45^\circ$ , but the relationships we derive are general; (b) shows the equivalent situation for a square plate on the sphere. In the traditional descriptions,  $\vec{F}_n$  is associated with a torque ( $\tau$ ) around Earth's centre, as in Eq. 5. This torque vector has components in the  $x$ ,  $y$ , and  $z$  directions. The  $z$  direction is aligned with the vector that points radially outward at the plate centroid ( $\hat{r}_c$ ). We refer to the component of the torque in the  $z$  (or  $\hat{r}_c$ ) direction, as the radial component of the torque; this is the true torque component, which is analogous to the usual definition of the torque as in case (a). For small plates (where the small angle approximation for  $\varphi$  is valid), the descriptions of the mechanics in (a) and (b) are identical, as discussed in the main text.

288 In addition, Fig. 5 shows the orientation of a putative boundary-normal collision  
 289 resistance force at Zealandia (shown schematically with the red arrow). To simplify the  
 290 figure, we have not shown the full decomposition of this point force, but only the pro-  
 291 jection of the point force onto the hemispheric plane (also with a red arrow). This ev-  
 292 idences the capacity for a plate boundary normal force at the Zealandia margin to pro-  
 293 duce a radial component of torque, primarily because angle between the centroid direc-  
 294 tion and the boundary normal (i.e.  $\theta$ ) is large. The key insight from Fig. 5 is that plate  
 295 boundary normal forces acting along both the IBM and Zealandia margins, are expected  
 296 to be relatively effectively partitioned into the radial component of the torque on the Pa-  
 297 cific Plate. In addition, the radial torque components are complimentary – both having  
 298 a CCW sign (when looking down on the Pacific centroid). In fact, these two boundaries  
 299 act in the sense of a force couple, as the tangential torque component of collision resis-  
 300 tance along the Zealandia margin would tend to oppose the tangential component of torque  
 301 due to the IBM margin.

### 302 3.3 Assumptions in the estimation of torque components

303 Having discussed the general aspects of torques due to plate boundary forces, we  
 304 conclude this section with some methodological details in applying this framework to plate  
 305 reconstruction models. In this study we restrict our attention to putative plate bound-  
 306 ary normal forces that arise from Pacific Plate subduction margins, as well as the po-  
 307 tential collision resistance from the intra-continental Zealandia margin.

308 Eq. 6 provides a means of calculating the radial and tangential components of the  
 309 torque, in a rotated reference frame, which is instructive for understanding torque par-  
 310 titioning due to a point force. However, for the general analysis we simply calculate a  
 311 net torque ( $\tau_{net}$ ) as the sum of torque increments in a fixed Cartesian coordinate sys-  
 312 tem (as in Eq. 4). The radial and tangential components are calculated using projec-  
 313 tions onto the centroid vector (identical to Eq. 1 for the rotation vector). We compute  
 314 the torque components both in terms of the net Pacific Plate subduction margin torque,  
 315 and at the level of regional margin segments (e.g. IBM, Tonga, Aleutian etc.). The lo-  
 316 cation and extent of these regional segments, at several times, is shown in Supplemen-  
 317 tary Fig. S4.

318 The analysis does not account for the age of the subducting plate in terms of the  
 319 predicted slab pull force, and is purely based on geometric information. In keeping with  
 320 this assumption, the calculations are based on the geometric centroid of the Pacific Plate,  
 321 rather than attempting to estimate the center of mass. The centroid locations are shown  
 322 in Fig. 1, and remain relatively stationary across the Cenozoic. The torque values in Fig.  
 323 6 are non-dimensionalised by assuming a reference torque  $\tau_{ref} = F_n R_e^2$ . The torque  
 324 calculations (e.g Eq. 3) are scaled by  $\tau_{ref}$ , such that the magnitude of  $F_n$  is not actu-  
 325 ally specified in our calculations. Hence, the estimated torque values discussed in the fol-  
 326 lowing section (e.g. Fig. 6) represent geometric information only.

327 In the reconstruction of Müller et al. (2016), the IBM subduction margin appears  
 328 at 55 Ma. However, geological evidence from the age and composition of initial magma-  
 329 tism, both in forearc and backarc regions, places the initiation age somewhat later at ca.  
 330 52 Ma (Ishizuka et al., 2006, 2011; Arculus et al., 2015). This issue has been highlighted  
 331 in the recent study of Hu et al. (2022b), which focuses on the drivers of the rapid change  
 332 in the azimuth of the Pacific plate (effectively the tangential part of the rotation). That  
 333 study proposes that: 1) the IBM initiation probably occurs somewhat later than the Müller  
 334 et al. (2016) model represents; and 2) the development of a slab pull force is delayed for  
 335 a further several million years, representing the time taken for the accumulating upper  
 336 mantle slab density to begin to dominate over forces resisting subduction (such as bend-  
 337 ing, interplate friction etc.)

338 In light of these insights, our subduction margin analysis makes the following as-  
 339 sumptions: Firstly, we use an updated plate geometry model (Hu et al., 2022b), which  
 340 is based on the Müller et al. (2016) model, but includes additional north-dipping Pacific  
 341 Plate subduction prior to 47 Ma (the Kronostsky margin). Secondly, we delay the IBM  
 342 initiation time to 52 Ma. Thirdly, we introduce a lag phase of 5 Ma, such that forces as-  
 343 sociated with new subduction margins do not immediately act on the trailing (e.g. Pa-  
 344 cific) plate. This applies to all initiating subduction zones across the Cenozoic. Our anal-  
 345 ysis only includes ‘outward’ Pacific Plate subduction margin segments; where other plates  
 346 subduct inward under the Pacific Plate (such as the Puysegur margin, south of New Zealand)  
 347 these are not included in the torque calculation.

348 To estimate the torque contributions due to collision resistance at the Zealandia  
 349 margin, we have made a few further simplifying assumptions. We assume collision res-  
 350 sistance forces ( $F_c$ ), with a specified, constant magnitude operated throughout the pivot  
 351 period (ca. 47-32 Ma), before and after which they were absent. During the pivot pe-  
 352 riod, we model the collisional Zealandia margin as a 1000 km segment which is perfectly  
 353 parallel to the centroid direction. This means that the plate boundary normal force is  
 354 orthogonal to the centroid direction, or  $\theta = 90^\circ$  (see Fig. 5). The length of intra-continental  
 355 boundary, parallel to the centroid direction, is on the order of 1000 km, as shown in Sup-  
 356 plementary Figure S5. Under these assumptions (e.g.  $\theta = 90^\circ$ ), the 47 Ma intra-continental  
 357 Zealandia margin, has a radial/tangential ratio of  $\sim 1.5$  (from Eq. 6 this ratio is equal  
 358 to  $\cos(\varphi)/\sin(\varphi)$ , and corresponds to  $\varphi$  of  $56^\circ$ ). The implication is that the Zealandia  
 359 margin would have predominantly partitioned plate boundary normal forces into a (CCW)  
 360 radial torque component.

361 In the following sections we will refer to the magnitude of plate boundary force den-  
 362 sities (forces per unit length, e.g., TN/m) that arise from subduction margins as  $F_{sp}$ , and  
 363 those that arise from the Zealandia collisional margin as  $F_c$ . We denote the ratio of these  
 364 force densities as  $F_R = F_c/F_{sp}$ .

## 365 4 Results

### 366 4.1 Evolution of Pacific Plate torque components

367 Fig. 6 shows the radial and tangential torque components, associated with Pacific  
 368 Plate subduction margins, and Zealandia margin collision, based on assumptions discussed  
 369 in the previous section. The solid black lines in Fig. 6 show the estimated net subduction-  
 370 related torque components, while the colored circles show the contributions of individ-  
 371 ual subduction margins (e.g., IBM, Tonga, etc.). Several new subduction margins ini-  
 372 tiate prior to the Eocene transition, (IBM, Japan and Kurile) as shown in Fig. 6A. This  
 373 is reflected in a significant increase in the magnitude of the tangential torque component  
 374 between about 55-47 Ma, shown with the solid black line in Fig. 6B. For the remainder  
 375 of the Cenozoic, the predicted magnitude of the tangential torque component remains  
 376 quite stable, with an average dimensionless value of around 1.4.

377 Fig. 6B reveals that the tangential component of the subduction margin torques  
 378 are broadly constructive, as shown by the fact that the magnitude of net tangential torque  
 379 is usually significantly larger than any of the individual regional components. However,  
 380 also note that the total tangential torque (solid black line Fig. 6B) is the *vector sum* of  
 381 the boundary contributions, it is not the sum of the magnitudes of the regional segments  
 382 (which is shown with the thin black line). The difference between the solid and dashed  
 383 lines represents the level destructive interference, typically amounting to about  $\frac{1}{3}$  of the  
 384 total, and varying somewhat over time. An example of the vector nature of the torque  
 385 contributions is given by the cessation of the Melanesian subduction which occurs at ca.  
 386 12 Ma. The cessation of subduction along this margin is calculated to have had very lit-  
 387 tle impact on the magnitude of the total tangential torque (thick black line), because the

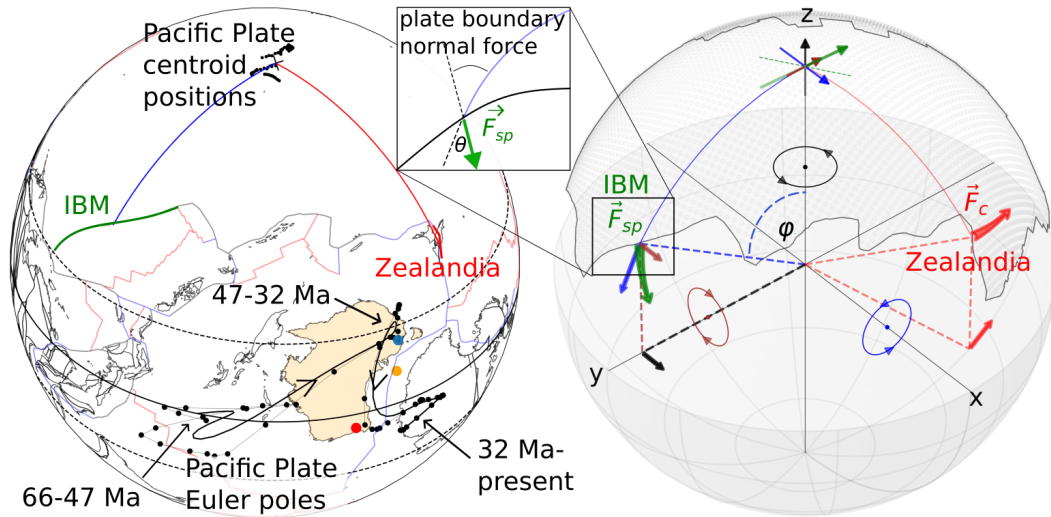


**Figure 5.** Schematic showing how different torque components are generated from plate boundary forces. Both panels show the tectonic configuration at 47 Ma. Globe is rotated so that the Pacific centroid lies at the pole (along the  $z$ -axis) while the arc from the centroid to the IBM margin lies in  $y$ - $z$  plane. Left panel shows the Pacific Plate Euler poles relative to the reference frame (black points). The right panel shows a schematic representation of plate boundary normal forces, for subduction at the IBM margin (green) and collision resistance at Zealandia margin (red). The blue, brown and black arrows show how the point force normal to the IBM margin would contribute to three orthogonal torques. The component of the point force acting in the centroid direction (in the same plane as the  $y$ -axis) produces a torque around the  $x$ -axis (blue symbols). This is a pseudo-torque because it has no dependence in the angle  $\varphi$ . The component of the force orthogonal to the centroid direction produces a radial torque (a ‘true’ torque) around the  $z$ -axis (or centroid axis). Both the IBM and Zealandia margins are expected to produce significant CCW radial torques on the Pacific Plate.

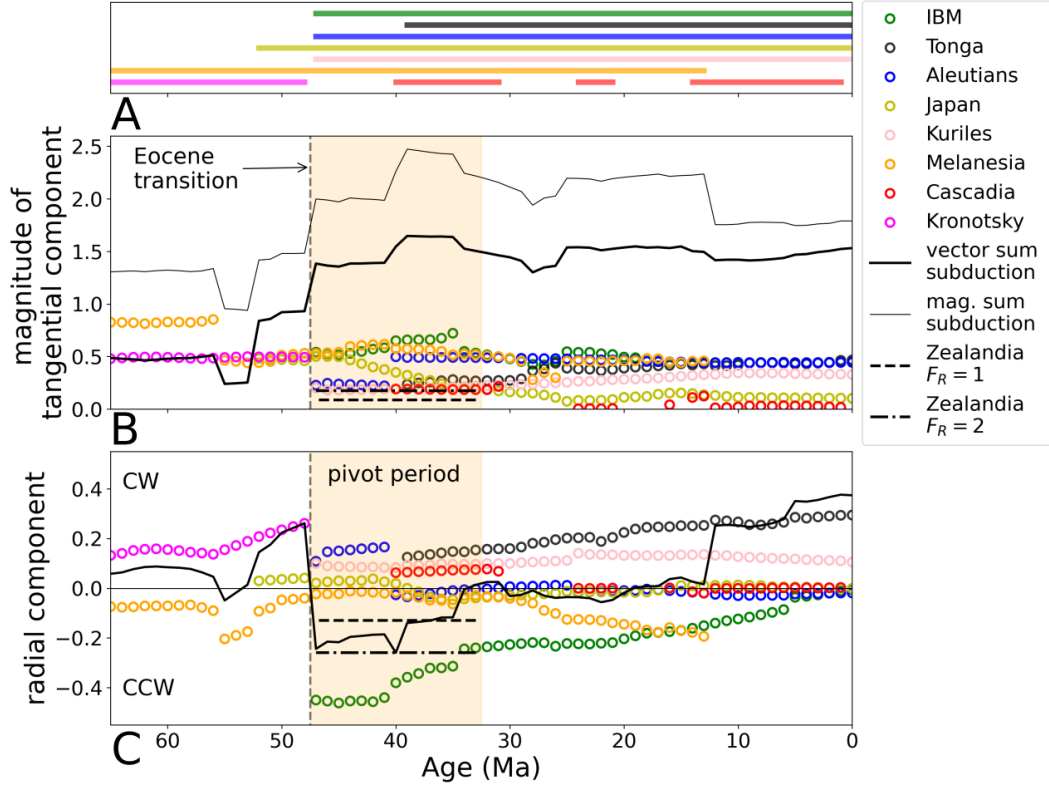


**Figure 6.** Evolution of torque components due to Pacific Plate subduction margin forces, based on the plate reconstruction model of Müller et al. (2016), incorporating an updated Pacific subduction margin model of Hu et al. (2022b). Torque values are dimensionless, as discussed in the main text. Colored circles show the contribution of regional subduction zones, such as the IBM margin, as labelled in the legend. The top panel (A) shows the duration of the regional subduction segments. (B) shows the magnitude of the tangential torque components. The vector sum of the regional torque contributions is shown with a solid black line, while the dashed black line is the sum of the magnitudes of the regional torque contributions. (C) shows radial torque components; in this case the vector sum (solid black line) is equal to the sum of the magnitudes of regional contributions, because the radial torque components are always parallel. Also shown here are the estimated contributions of the Zealandia margin, during the pivot period, under 2 assumptions about the relative ratio of collision to subduction-related force densities, as discussed in Section 3.3.  $F_R=1$  is shown with the thick dashed line, and where Zealandia collisional forces were assumed to be equal the magnitude of subduction-related forces.  $F_R=2$  is shown with the thick dot-dashed line, where collisional forces are twice the magnitude of subduction margin forces.

388 south-dipping orientation of the Melanesian margin produced a regional torque contri-  
 389 bution that was near-perpendicular to the total torque (see Supplementary Fig. S4). How-  
 390 ever the cessation of subduction is clearly evident in the sum of magnitudes of the re-  
 391 gional torque contribution (thin black line).

392 Fig. 6C shows the radial component of the estimated torques acting on the Pacific  
 393 Plate. There are two key insights we draw from this plot. First is that the IBM margin  
 394 – during the pivot period – has the largest predicted radial torque contribution of any  
 395 regional segment of the subduction margin at any time throughout the Cenozoic. Dur-  
 396 ing this peak, the radial component of the IBM margin is more than twice the magni-  
 397 tude of the next largest regional component (Aleutian margin), and exhibits a maximum  
 398 radial/tangential torque ratio of  $\sim 0.9$  (i.e. almost equal partitioning). Secondly, the es-  
 399 timated radial torque components tend to exhibit significant destructive interference (in  
 400 contrast to the tangential torques). For instance, the net radial torque is close to zero  
 401 in the interval ca. 32-12 Ma, due to the opposing radial torque contributions of individ-  
 402 ual segments, such as IBM (CCW) and Tonga (CW) margins. This attribute of the ra-  
 403 dial torque contributions has implications for the relative impact of additional forces, such  
 404 as from the Zealandia margin. Overall, there is a broad trend from a CCW radial com-  
 405 ponent beginning at the Eocene transition, when the IBM margin dominated the radial  
 406 torque, to a CW rotation torque component during the past ca. 12 Myr, where Tonga  
 407 dominates. Note that progressive, differential, trench rollback in these 2 segments has  
 408 followed an opposite trajectory, as far as the magnitude of the radial torque is concerned.  
 409 Along the IBM margin, rollback has decreased the  $\theta$  angle, partitioning ever-less force  
 410 into the radial component of the torque, while the opposite is true for the Tonga mar-  
 411 gin.

412 The dashed and dot-dashed lines in Fig. 6 show the estimated torque contributions  
 413 for Zealandia, based on assumptions about the boundary geometry discussed in the pre-  
 414 vious section. Two cases are shown, 1: where the Zealandia margin force density is as-  
 415 sumed to be the same as that of the subduction margins (i.e.  $F_R = 1$ , dashed line), and  
 416 2: where the Zealandia margin is 2 times larger than the latter (i.e.  $F_R = 2$ , dot-dashed  
 417 line). Under either assumption, the contribution of Zealandia to tangential torques is sig-  
 418 nificantly smaller than the net effect of subduction margins. This point will also be seen  
 419 in Fig. 7, where we consider the (vector) addition of the torque components due to Zealan-  
 420 dia and the net torque due to subduction. The simple conclusion is that under the as-  
 421 sumptions represented in Figs. 6&7, Zealandia does not amount to a first-order contri-  
 422 bution in terms of the tangential torque.

423 In terms of radial torques, the impact of Zealandia may be much more significant.  
 424 Indeed, we see that the two respective assumptions about  $F_R$  (dashed and dot-dashed  
 425 lines, in Fig. 6) lead to radial torque contributions that bound the net radial torque con-  
 426 tribution of the subduction margins (shown with a solid black line). Note, however, that  
 427 even under the stronger assumption about collisional forces ( $F_R = 2$ ), the IBM mar-  
 428 gin is still the largest single contributor to radial torques. This is because the IBM mar-  
 429 gin is about 4.5 times longer than the assumed length of the Zealandia margin (1000 km).  
 430 However, the radial torque contribution of the IBM margin is buffered the tendency of  
 431 most other subduction margins to pull in a CW sense. The destructive interference in  
 432 radial subduction torques amplifies the contribution of the Zealandia margin.

## 433 4.2 Comparison of torques and Pacific Plate motion changes

434 Fig. 7 shows a comparison between rotation components (in green) and dimension-  
 435 less torques (in black). The vertical scales have been arbitrarily chosen so that the ro-  
 436 tations (left axis) and torques (right axis) have similar total variation. In examining po-  
 437 tential correlations, it is important to consider the geodynamic framework discussed in  
 438 the final paragraph of the introduction, regarding the drivers of rapid plate motion changes.

439 A specific implication of this framework is that torques due to subduction and collision  
 440 represent only a partial description of the overall plate equilibrium. Therefore, we would  
 441 not expect perfect alignment between plate rotation vectors and torque vectors due to  
 442 subduction/collision. However, we would expect to see an overall consistency between  
 443 rapid changes in subduction/collision torques and similarly-rapid changes in rotation.  
 444 For, instance, if torque changes imply a CW change in the plate azimuth at the centroid,  
 445 we would expect a similar CW change in plate rotation, although both the absolute val-  
 446 ues and the relative magnitude of the change may differ, which would represent the pres-  
 447 ence of additional forces in the overall plate equilibrium. In Fig. 7A, we can see that prior  
 448 to the Eocene transition, the azimuth of the Pacific Plate is poorly predicted by subduc-  
 449 tion related torques (e.g. Fig. 7A). This is despite inclusion (in our calculations) of an  
 450 updated model for northern Pacific Plate subduction margins (Hu et al., 2022b). This  
 451 lack of correlation, however, may simply represent the fact that additional forces, e.g.  
 452 due to long-wavelength flow, provided a northerly-oriented force component. Indeed this  
 453 is the explanation advanced by previous studies, which have noted a similar mismatch  
 454 in this time period (Faccenna et al., 2012). The numerical model results, which we dis-  
 455 cuss later in this section, support this interpretation.

456 Figure. 7 suggests that there two Cenozoic events (47 Ma and 12 Ma), in which  
 457 we see consistent changes between components of Pacific Plate rotation and subduction  
 458 torques. We have already commented on the subduction-margin reconfiguration that oc-  
 459 curred prior to the Eocene transition, including initiation of the IBM subduction zone.  
 460 Changes in estimated subduction torque at 47 Ma, are consistent with the sign of the  
 461 changes in rotation components. However, the radial component exhibits the clearest cor-  
 462 relation, in that both the sign and relative magnitude of the change exhibit closer sim-  
 463 ilarity: in each case, the Eocene transition represents the single largest radial change across  
 464 the Cenozoic.

465 The change in torque components at about 12 Ma is associated with the cessation  
 466 of southward dipping subduction at Melanesia. The geodynamic context is the collision  
 467 of the Ontong Java Plateau, potential slab breakoff and subduction polarity reversal. A  
 468 previous study, based on dynamic modelling, has proposed a link between the collision  
 469 and the observed northwards change in Pacific Plate velocities in this period (although  
 470 it was based on a plate reconstruction that puts the timing of the collision somewhat later  
 471 (Austermann et al., 2011)). Our analysis provides the additional insight that this change  
 472 involved both the tangential azimuth (Fig. 7A) and, to an even greater (relative) degree,  
 473 the radial rotation component of rotation/torque (Fig. 7C). The only component of this  
 474 ca. 12 Ma change that is not consistent, in terms plate rotation versus torque estimates,  
 475 is the magnitude of the tangential change (Fig. 7B). However, in both cases changes in  
 476 this component are small compared to the relative change in the other 2 components.  
 477 Hence we view this inconsistency as being of minor importance.

478 Overall, however, there remain several aspects of Cenozoic Pacific Plate rotation  
 479 which are not correlated with patterns in estimated torques. Importantly, this includes  
 480 instances of rotation changes that are rapid in nature. For instance, consider the rapid  
 481 decrease (and reversal) of the CCW radial rotation component at the end of the pivot  
 482 period (ca. 32 Ma) shown in green line Fig. 7C. While subduction torques predict a de-  
 483 crease in the CCW component across the pivot period, the rapid nature of this change  
 484 is not predicted.

485 Furthermore, subduction-related torques do not provide an explanation for many  
 486 of the rapid changes in the magnitude of the tangential component of Pacific Plate ve-  
 487 locity (Fig. 7B), such as those which occur at ca. 60, 40, & 28 Ma. The change in tan-  
 488 gential rotation magnitude, at 40 Ma, is worth highlighting as it exhibits neither a cor-  
 489 responding change in the azimuth of the plate at the centroid (Fig. 7A), nor in the ra-  
 490 dial rotation component (Fig. 7C). This represents a case of a reduction in the tangen-  
 491 tial rotation rate, but negligible change in the rotation axis. These changes would seem

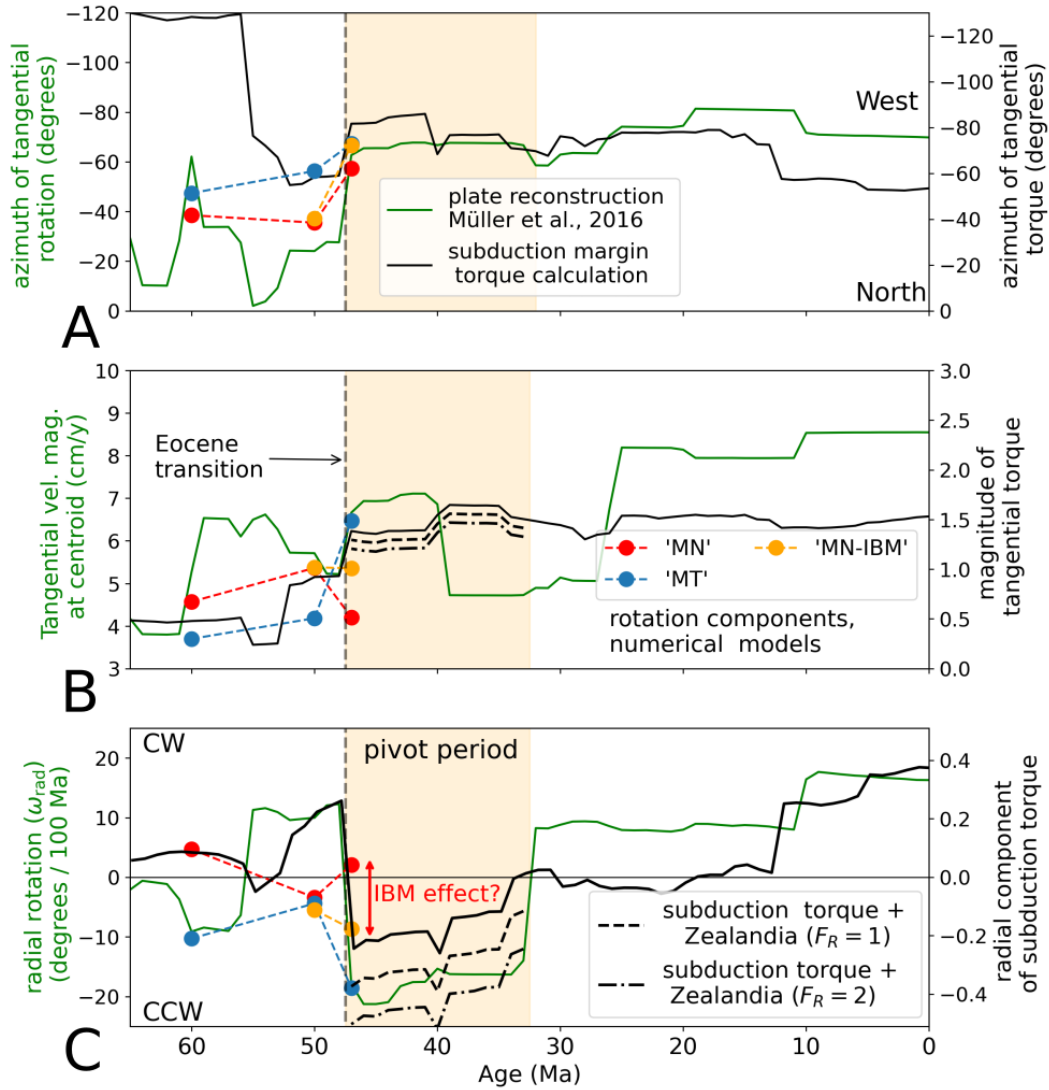


**Figure 7.** Comparison between estimated subduction related torques and components of the Pacific Plate rotation vector. Green line show plate rotation components as based on Müller et al. (2016)(see Fig. 3 caption for further details). Net subduction torque components are shown with solid black lines, as in Fig. 6. The dashed and dot-dashed line segments show estimated torque contributions of the Zealandia margin, added to the total subduction related torques. Zealandia opposes the tangential torque of the subduction margins, but compliments the CCW radial rotation. Two scenarios are shown,  $F_R=1$ , and  $F_R=2$ , as discussed in Section 4. The colored circles show rotation components from global-scale numerical models of Hu et al. (2022b). The difference between the ‘MN’ and ‘MN-IBM’ models provides an estimate of the effect of the IBM margin. This is shown with the vertical red arrow, labelled ‘IBM effect?’ in the bottom panel (C). The corresponding difference in azimuth (top panel) is less significant (as discussed in Hu et al. (2022b)).

492 to imply a slowdown of the system, while the relative magnitudes of driving/resisting  
 493 forces remain constant (hence no shift in the rotation axis). Our analysis suggests there  
 494 is nothing in the evolving geometry of the Pacific Plate subduction margin that could  
 495 account for this change. Moreover, rapid changes in regional subduction margins tend  
 496 to produce changes in plate direction and/or radial rotation (47 Ma and 12 Ma). While  
 497 rapid changes in plate motion are often attributed to the rapid evolution of subduction  
 498 margins, it seems difficult to account for the 40 Ma slowdown in that context.

499 Subduction margin-related torque changes can provide an explanation for some –  
 500 but not all – of the rapid changes in Cenozoic Pacific Plate motion (as represented in  
 501 plate reconstruction models of Müller et al. (2016)). Fig. 7 also shows how putative col-  
 502 lisional forces along the Eocene Zealandia margin might have impacted the torque bal-  
 503 ance. In evaluating the potential contribution, there are two basic questions to assess:  
 504 1) is it plausible that collision resistance forces along the Zealandia margin could have  
 505 a first order impact on Pacific Plate torques? And 2: does the nature of these torques  
 506 contributions have explanatory power in terms of observed rotations? Note that in Fig.  
 507 7, we show the effect of Zealandia margin forces under the assumptions that such forces  
 508 operated with a constant magnitude within the pivot period, but were otherwise absent.  
 509 This is, of course, a major simplification. However, our approach is intended simply to  
 510 assess the relative capacity of the Zealandia margin to affect Pacific Plate torques dur-  
 511 ing the pivot period.

512 As previously discussed, the assumption of  $F_R = 1$ , already implies that Zealan-  
 513 dia would have had a first-order effect on the radial component of Pacific Plate torques,  
 514 relative to the net subduction component.  $F_R$  of  $\sim 2$ , makes the total (subduction plus  
 515 collision) radial torque during the pivot period higher than at any other stage during the  
 516 Cenozoic; this assumption can therefore account for the similar peak in radial rotation  
 517 rate. A further assumption – that Zealandia collision resistance rapidly reduced at around  
 518 32 Ma – helps to explain the rapid reduction in the (CCW) radial rotation at the  
 519 end of the pivot period, which subduction margin forces alone cannot account for. Dur-  
 520 ing this period, the Zealandia margin evolves from the stage of pivoting, where the Pacific-  
 521 Australian Euler pole lay on the plate boundary (Sutherland, 1995), to a mature trans-  
 522 form boundary, as Zealandia moved NW away from the Euler pole (as viewed relative  
 523 to the absolute reference frame, e.g. Fig. 2). During such an evolution, it is conceivable  
 524 that a rapid change in boundary-normal forces – an kind of unlocking process – may have  
 525 occurred. However, such a transition (at about 32 Ma) is speculative, and should be con-  
 526 sidered as such.

### 527 4.3 Insights from global geodynamic models

528 Even when modified to try to better represent dynamic process (such as a subduc-  
 529 tion initiation lag), the use of parameterised plate boundary forces has obvious limita-  
 530 tions (Becker & O’Connell, 2001). The results from global-scale numerical models pro-  
 531 vide an alternative opportunity to establish potential links between evolving plate bound-  
 532 aries, and plate motion changes. A recent example of this approach is demonstrated in  
 533 Hu et al. (2022b), which compares two alternative models for the subduction boundary  
 534 evolution of the Pacific Plate.

535 The reference model (‘MT’) presented in Hu et al. (2022b) is based on the plate  
 536 reconstruction of Müller et al. (2016), while an alternative model (‘MN’) includes a several-  
 537 thousand kilometer north-dipping intra-oceanic ‘Kronotsky’ subduction, which is active  
 538 until 50 Ma. This alternative model is run both with (‘MN-IBM’) and without (‘MN’)  
 539 subduction at the IBM margin. It should be noted that in all cases, the lithospheric struc-  
 540 ture includes the new Pacific-Australian plate boundary through Zealandia (from 47 Ma).  
 541 The models can, in principle, accommodate deformation and collision resistance across  
 542 the Zealandia margin. However, the models do not include features such as a strong, buoy-

543 ant, underthrust Hikurangi Plateau, which could limit how accurately they will capture  
 544 collision resistance across such a boundary (e.g., Reyners, 2013). Surface velocity fields  
 545 for the models of Hu et al. (2022b) were provided in the original study, from these we  
 546 estimated Euler poles based on least squares fitting. Based on these results we make the  
 547 following observations:

- 548 1. In both models (MT and MN) the Pacific Plate exhibits a NW velocity azimuth  
 549 at 60 Ma ( $-40^\circ$ , e.g., Fig. 7A). This is nearly orthogonal to the calculated azimuth  
 550 based in the torque due to subduction-related normal forces, based on the same  
 551 plate reconstruction ( $-120^\circ$ ). We interpret this as suggesting that other driving  
 552 forces (along with direct slab pull) play an important role (as was suggested by  
 553 Faccenna et al. (2012) for times prior to about 60 Ma).
- 554 2. The inclusion of subduction along the IBM margin produces a significant CCW  
 555 effect on the radial component of the rotation. This observation is primarily de-  
 556 duced from the model setups that are identical except for the inclusion the IBM  
 557 margin (MN-IBM & MN: shown as yellow and red circles in Figs. 1&7). This dif-  
 558 ference in these models is represented by the red labelled arrow in Fig. 7C.
- 559 3. The change in the Pacific Plate Euler pole location at 47 Ma, due to the inclu-  
 560 sion of the IBM subduction zone (initiating at 5 Ma), is along an arc that points  
 561 almost directly towards Zealandia. This can be seen by comparing the Euler poles  
 562 shown with the red and yellow circles in Fig. 1.
- 563 4. When the IBM margin is not included, the Pacific plate at 47 Ma has negligible  
 564 radial rotational component (e.g. ‘MN’ model, red symbol in Fig. 7C). In this model,  
 565 there is no residual CCW ‘signal’ which might be identified with the effect of the  
 566 Zealandia margin, independent from the effect of subduction at the IBM margin.

567 In summary, the models of Hu et al. (2022b) suggest that: (1) Pacific Plate motion  
 568 is sensitive to the structure of the subduction margins, although other driving forces  
 569 may be equally important; (2) the inclusion of subduction initiation at the IBM mar-  
 570 gin (at 51 Ma) has a relatively large impact on the radial rotation component (at 47 Ma),  
 571 which is consistent with our geometric analysis; (3) The absolute motion changes induced  
 572 by the IBM margin would in turn seem to facilitate Pacific-Australian (relative) pivot-  
 573 ing, as they move the Pacific Plate Euler pole towards Zealandia.

## 574 5 Discussion and conclusions

575 This study is fundamentally concerned with the relative and absolute motions of  
 576 the Pacific and Australian plates, spanning the period of rapid tectonic reorganisation  
 577 at ca. 50 Ma (The Eocene transition). This transition involves the frequently-discussed  
 578 westwards change in Pacific Plate absolute motion. Another aspect, which has been com-  
 579 paratively overlooked, is that Pacific Plate rotation also developed a relatively high ra-  
 580 dial component (CCW sense). Moreover, this period of high radial rotation (ca. 47 - 32  
 581 Ma, as inferred in Müller et al. (2016)), overlaps a similar interval wherein the relative  
 582 Pacific-Australian rotation axis was situated within continental Zealandia (Sutherland,  
 583 1995). Altogether, this sequence of events suggests that forces originating at the Zealan-  
 584 dia margin could have played an important role in the evolving Pacific Plate torque bal-  
 585 ance, along with those associated with the evolving subduction margin, which have been  
 586 a major focus of previous investigations (Whittaker et al., 2007; Faccenna et al., 2012;  
 587 Hu et al., 2022b).

588 Our torque analysis, along with results from numerical models, highlights the role  
 589 played by the IBM margin in the Eocene transition. In particular, the configuration of  
 590 the IBM margin leads to an anomalous impact on the radial component of torques (and  
 591 rotations in the case of the numerical models of Hu et al. (2022b)). This radial contri-  
 592 bution of the IBM has not been recognised in previous studies, which have – in a sense

593 – underestimated its overall importance (Hu et al., 2022b). Because of its geometric con-  
 594 figuration, Zealandia is even more efficient in terms of partitioning plate boundary nor-  
 595 mal forces into CCW radial torques. Hence, Zealandia provides a ‘push in the right di-  
 596 rection’. While both the IBM and Zealandia margins have strong potential for explain-  
 597 ing the CCW radial components of Pacific Plate rotation, additional assumptions are  
 598 required to make definitive statements about the relative contributions. In this study,  
 599 such assumptions are encapsulated in the value of  $F_R$ , being the relative force density  
 600 of collision resistance versus typical subduction margins. We show that  $F_R \sim 1$  is suf-  
 601 ficient for Zealandia to represent a first order contribution to the radial component of  
 602 the Pacific Plate torque balance. In Section 4, we posed the question is this ( $F_R \sim 1$ )  
 603 a plausible value?

604 Investigations in numerous settings have concluded that collisional margins may  
 605 produce force densities larger than typical subduction related forces (England & House-  
 606 man, 1986; Cloetingh & Wortel, 1986; England & Molnar, 2022; Reynolds et al., 2002).  
 607 Many such estimates relate to regions of significant crustal thickening, and associated  
 608 gravitational potential energy forces (e.g. Himalaya/Tibet, Andes); hence the applica-  
 609 bility with the Eocene Zealandia margin might be limited. However, significant Eocene  
 610 shortening and uplift are recorded in Zealandia, such as  $\sim 12$ -15 km of motion of the Taranaki  
 611 Fault beginning around 40–43 Ma (Stagpoole & Nicol, 2008), as well as the distributed  
 612 deformation of Zealandia that has recently been documented (Sutherland et al., 2020).  
 613 Hence regional geological evidence is consistent with significant deviatoric compression  
 614 across the northern part of Zealandia. We also note that the modern day Zealandia mar-  
 615 gin (Alpine Fault - Southern Alp System) is thought to transmit margin normal force  
 616 densities of about 3 TN/m (Reynolds et al., 2002; Sandiford et al., 2004), i.e. of simi-  
 617 lar magnitude to inferred net slab pull in several previous studies (Forsyth & Uyeda, 1975;  
 618 Schellart, 2004; Bird et al., 2008; Copley et al., 2010; England & Molnar, 2022). Over-  
 619 all, the proposition of equivalent force densities between subduction margins and colli-  
 620 sional margins is certainly plausible in terms of additional tectonic settings.

621 As we have shown, both radial and tangential changes in absolute Pacific Plate mo-  
 622 tion appear to have facilitated relative Pacific-Australian Euler poles locating close to  
 623 Zealandia during the pivot period. Boundary normal forces along Zealandia have rela-  
 624 tively little impact on the Pacific Plate tangential torques, compared to the integrated  
 625 effect of subduction margins. Our analysis suggests that the onset of Pacific-Australian  
 626 pivoting (at ca. 47 Ma) was tied to broader changes in the plate driving/resisting forces,  
 627 including far-field subduction zone reconfiguration, rather than being dominated by forces  
 628 arising proximal to the pivot point, i.e. collision resistance within the intra-continental  
 629 Zealandia margin. Nevertheless, it is plausible that forces along the Zealandia margin  
 630 played a contributing role in the anomalously high Pacific Plate radial rotation during  
 631 the pivot period. Moreover, rapidly evolving forces in the Zealandia margin, could help  
 632 to explain features that are not readily explicable in terms of subduction torques alone,  
 633 such as the rapid decline in radial rotation at about 32 Ma. This suggestion remains spec-  
 634 ulative however, and will require further analysis. Important insights may be gained from  
 635 analysing global convection models, such as those presented by Hu et al. (2022b), in terms  
 636 of a radial/tangential rotation decomposition.

## 637 6 Open Research

638 Data: Velocity grids from numerical models of (Hu et al., 2022b) are available at Cal-  
 639 tech Data (<https://doi.org/10.22002/D1.2150>) (Hu et al., 2022a)  
 640 Software: Geographical figures were made with GPlately (<https://doi.org/10.1002/gdj3.185>) (Mather et al., 2023).  
 641

642 **Acknowledgments**

643 PyGplates and gplately (Mather et al., 2023) software (www.gplates.org) are funded by  
644 the AuScope infrastructure-development programme. The work was supported by Aus-  
645 tralian Research Council grants DP150102887 and DP180102280. The research was fa-  
646 cilitated by the flexible and supportive Post Doctoral position provided by Monash Uni-  
647 versity and the aforementioned grants. We would like to thank Dr. Bernhard Steinberger  
648 as well as an anonymous reviewer for their constructive comments and attention to de-  
649 tail.

## References

- 650
- 651 Arculus, R. J., Ishizuka, O., Bogus, K. A., Gurnis, M., Hickey-Vargas, R., Aljahdali,  
652 M. H., . . . others (2015). A record of spontaneous subduction initiation in the  
653 izu–bonin–mariana arc. *Nature Geoscience*, *8*(9), 728–733.
- 654 Austermann, J., Ben-Avraham, Z., Bird, P., Heidbach, O., Schubert, G., & Stock,  
655 J. M. (2011). Quantifying the forces needed for the rapid change of pacific  
656 plate motion at 6 ma. *Earth and Planetary Science Letters*, *307*(3-4), 289–  
657 297.
- 658 Becker, T. W., & O’Connell, R. J. (2001). Predicting plate velocities with mantle  
659 circulation models. *Geochemistry, Geophysics, Geosystems*, *2*(12).
- 660 Bird, P., Liu, Z., & Rucker, W. K. (2008). Stresses that drive the plates from below:  
661 Definitions, computational path, model optimization, and error analysis. *Journal of Geophysical Research: Solid Earth*, *113*(B11).
- 662 Cloetingh, S., & Wortel, R. (1986). Stress in the indo-australian plate. *Tectono-*  
663 *physics*, *132*(1-3), 49–67.
- 664 Colli, L., Stotz, I., Bunge, H.-P., Smethurst, M., Clark, S., Iaffaldano, G., . . .  
665 Bianchi, M. C. (2014). Rapid south atlantic spreading changes and coeval  
666 vertical motion in surrounding continents: Evidence for temporal changes of  
667 pressure-driven upper mantle flow. *Tectonics*, *33*(7), 1304–1321.
- 668 Copley, A., Avouac, J.-P., & Royer, J.-Y. (2010). India-asia collision and the ceno-  
669 zotic slowdown of the indian plate: Implications for the forces driving plate  
670 motions. *Journal of Geophysical Research: Solid Earth*, *115*(B3).
- 671 Eberhart-Phillips, D., Reyners, M., Upton, P., & Gubbins, D. (2018). Insights into  
672 the structure and tectonic history of the southern south island, new zealand,  
673 from the 3-d distribution of p-and s-wave attenuation. *Geophysical Journal*  
674 *International*, *214*(2), 1481–1505.
- 675 England, P., & Houseman, G. (1986). Finite strain calculations of continental deforma-  
676 tion: 2. comparison with the india-asia collision zone. *Journal of Geophysical*  
677 *Research: Solid Earth*, *91*(B3), 3664–3676.
- 678 England, P., & Molnar, P. (2022). Changes in plate motions caused by increases  
679 in gravitational potential energy of mountain belts. *Geochemistry, Geophysics,*  
680 *Geosystems*, *23*(10), e2022GC010389.
- 681 Faccenna, C., Becker, T. W., Lallemand, S., & Steinberger, B. (2012). On the role of  
682 slab pull in the cenozoic motion of the pacific plate. *Geophysical Research Let-*  
683 *ters*, *39*(3).
- 684 Forsyth, D., & Uyeda, S. (1975). On the relative importance of the driving forces of  
685 plate motion. *Geophysical Journal International*, *43*(1), 163–200.
- 686 Gaina, C., Müller, D. R., Royer, J.-Y., Stock, J., Hardebeck, J., & Symonds, P.  
687 (1998). The tectonic history of the tasman sea: a puzzle with 13 pieces. *Journal of Geophysical Research: Solid Earth*, *103*(B6), 12413–12433.
- 688 Gurnis, M. (2023). An evolutionary perspective on subduction initiation. In *Dynam-*  
689 *ics of plate tectonics and mantle convection* (pp. 357–383). Elsevier.
- 690 Hu, J., Gurnis, M., Rudi, J., Stadler, G., & Müller, R. D. (2022a). Data set for  
691 manuscript ”dynamics of the abrupt change in pacific plate motion around 50  
692 ma” [dataset].  
693 doi: 10.22002/D1.2150
- 694 Hu, J., Gurnis, M., Rudi, J., Stadler, G., & Müller, R. D. (2022b). Dynamics of  
695 the abrupt change in pacific plate motion around 50 million years ago. *Nature*  
696 *Geoscience*, *15*(1), 74–78.
- 697 Ishizuka, O., Kimura, J.-I., Li, Y. B., Stern, R. J., Reagan, M. K., Taylor, R. N., . . .  
698 others (2006). Early stages in the evolution of izu–bonin arc volcanism: New  
699 age, chemical, and isotopic constraints. *Earth and Planetary Science Letters*,  
700 *250*(1-2), 385–401.
- 701 Ishizuka, O., Tani, K., Reagan, M. K., Kanayama, K., Umino, S., Harigane, Y., . . .  
702 Dunkley, D. J. (2011). The timescales of subduction initiation and subse-

- 705           quent evolution of an oceanic island arc. *Earth and Planetary Science Letters*,  
706           306(3-4), 229–240.
- 707 Keller, W. R. (2005). *Cenozoic plate tectonic reconstructions and plate boundary*  
708           *processes in the southwest pacific*. California Institute of Technology.
- 709 Lamb, S., Mortimer, N., Smith, E., & Turner, G. (2016). Focusing of relative plate  
710           motion at a continental transform fault: Cenozoic dextral displacement, 700  
711           km on new zealand’s alpine fault, reversing, 225 km of late cretaceous sinistral  
712           motion. *Geochemistry, Geophysics, Geosystems*, 17(3), 1197–1213.
- 713 Mahoney, J., Storey, M., Duncan, R., Spencer, K., & Pringle, M. (1993). Geochem-  
714           istry and age of the ontong java plateau. *The mesozoic Pacific: Geology, tec-*  
715           *tonics, and volcanism*, 77, 233–261.
- 716 Mather, B. R., Müller, R. D., Zahirovic, S., Cannon, J., Chin, M., Ilano, L., . . . oth-  
717           ers (2023). Deep time spatio-temporal data analysis using pygplates with plate  
718           tectonic tools and gplatly. *Geoscience Data Journal*.
- 719 Morgan, W. J. (1972). Plate motions and deep mantle convection. *Geological Society*  
720           *of America Memoirs*, 132, 7–22.
- 721 Mortimer, N. (2018). Evidence for a pre-eocene proto-alpine fault through zealandia.  
722           *New Zealand Journal of Geology and Geophysics*, 61(3), 251–259.
- 723 Müller, R. D., Seton, M., Zahirovic, S., Williams, S. E., Matthews, K. J., Wright,  
724           N. M., . . . others (2016). Ocean basin evolution and global-scale plate reorga-  
725           nization events since pangea breakup. *Annual Review of Earth and Planetary*  
726           *Sciences*, 44(1), 107–138.
- 727 O’Connor, J. M., Hoernle, K., Müller, R. D., Morgan, J. P., Butterworth, N. P.,  
728           Hauff, F., . . . Stoffers, P. (2015). Deformation-related volcanism in the pa-  
729           cific ocean linked to the hawaiian–emperor bend. *Nature Geoscience*, 8(5),  
730           393–397.
- 731 Reyners, M. (2013). The central role of the hikurangi plateau in the cenozoic tecton-  
732           ics of new zealand and the southwest pacific. *Earth and Planetary Science Let-*  
733           *ters*, 361, 460–468.
- 734 Reynolds, S. D., Coblenz, D. D., & Hillis, R. R. (2002). Tectonic forces controlling  
735           the regional intraplate stress field in continental australia: Results from new fi-  
736           nite element modeling. *Journal of Geophysical Research: Solid Earth*, 107(B7),  
737           ETG–1.
- 738 Sandiford, M., Wallace, M., & Coblenz, D. (2004). Origin of the in situ stress field  
739           in south-eastern australia. *Basin Research*, 16(3), 325–338.
- 740 Schellart, W. (2004). Quantifying the net slab pull force as a driving mechanism for  
741           plate tectonics. *Geophysical research letters*, 31(7).
- 742 Stagpoole, V., & Nicol, A. (2008). Regional structure and kinematic history of  
743           a large subduction back thrust: Taranaki fault, new zealand. *Journal of Geo-*  
744           *physical Research: Solid Earth*, 113(B1).
- 745 Steinberger, B. (2000). Plumes in a convecting mantle: Models and observations for  
746           individual hotspots. *Journal of Geophysical Research: Solid Earth*, 105(B5),  
747           11127–11152.
- 748 Steinberger, B., Schmeling, H., & Marquart, G. (2001). Large-scale lithospheric  
749           stress field and topography induced by global mantle circulation. *Earth and*  
750           *Planetary Science Letters*, 186(1), 75–91.
- 751 Stotz, I., Iaffaldano, G., & Davies, D. R. (2018). Pressure-driven poiseuille flow:  
752           a major component of the torque-balance governing pacific plate motion. *Geo-*  
753           *physical Research Letters*, 45(1), 117–125.
- 754 Sutherland, R. (1995). The australia-pacific boundary and cenozoic plate motions in  
755           the sw pacific: Some constraints from geosat data. *Tectonics*, 14(4), 819–831.
- 756 Sutherland, R., Collot, J., Bache, F., Henrys, S., Barker, D., Browne, G., . . . oth-  
757           ers (2017). Widespread compression associated with eocene tonga-kermadec  
758           subduction initiation. *Geology*, 45(4), 355–358.

- 759 Sutherland, R., Dickens, G. R., Blum, P., Agnini, C., Alegret, L., Asatryan, G., . . .  
760 others (2020). Continental-scale geographic change across Zealandia during  
761 Paleogene subduction initiation. *Geology*, *48*(5), 419–424.
- 762 Torsvik, T. H., Müller, R. D., Van der Voo, R., Steinberger, B., & Gaina, C. (2008).  
763 Global plate motion frames: toward a unified model. *Reviews of Geophysics*,  
764 *46*(3).
- 765 Wessel, P., & Kroenke, L. W. (2008). Pacific absolute plate motion since 145 Ma:  
766 An assessment of the fixed hot spot hypothesis. *Journal of Geophysical Re-*  
767 *search: Solid Earth*, *113*(B6).
- 768 Whittaker, J., Muller, R., Leitchkov, G., Stagg, H., Sdrolias, M., Gaina, C., &  
769 Goncharov, A. (2007). Major Australian-Antarctic plate reorganization at  
770 Hawaiian-Emperor bend time. *Science*, *318*(5847), 83–86.